JOURNAL OF GEOPHYSICAL RESEARCH, VOL. ???, XXXX, DOI:10.1029/,

Spectral signatures of characteristic spatial scales and non-fractal structure in landscapes

J. Taylor Perron,[1] James. W. Kirchner,[2,3,4] and William E. Dietrich[2]

Abstract. Landscapes are sometimes argued to be scale-invariant or random surfaces, yet qualitative observations suggest that they contain characteristic spatial scales. We quantitatively investigate the existence of characteristic landscape scales by analyzing two-dimensional Fourier power spectra derived from high-resolution topographic maps of two landscapes in northern California. In both cases, we find that spectral power declines sharply above a frequency that corresponds roughly to hillslope length, implying that the landscape is relatively smooth at finer scales. The spectra also show that both landscapes contain quasiperiodic ridge-and-valley structures, and we derive a robust measure of the ridge-valley wavelength. By comparing the spectra with the statistical properties of spectra derived from randomly generated topography, we show that such uniform valley spacing is unlikely to occur in a random surface. We describe several potential applications of spectral analysis in geomorphology beyond the identification of characteristic spatial scales, including a filtering technique that can be used to measure topographic attributes, such as local relief, at specific scales or in specific orientations.

1. Introduction

Some properties of landscapes suggest that Earth's surface topography might be scale-invariant. Field observations and perusal of topographic maps lead to the qualitative impression that erosionally dissected landscapes have a similar appearance over a wide range of spatial scales [e.g., *Davis*, 1899; *Montgomery and Dietrich*, 1992]. Formal analyses of topographic data suggest that some landscapes may be either self-similar (consisting of landforms with the same shape and aspect ratio at every scale) or self-affine (aspect ratio varies with scale) [e.g., *Vening Meinesz*, 1951; *Mandelbrot*, 1975; *Sayles and Thomas*, 1978; *Church and Mark*, 1980; *Mandelbrot*, 1983; *Matsushita and Ouchi*, 1989; *Newman and Turcotte*, 1990; *Balmino*, 1993; *Turcotte*, 1997; *Rodríguez-Iturbe and Rinaldo*, 2001], or may display other properties of random or fractal surfaces [e.g., *Shreve*, 1966; *Ahnert*, 1984; *Culling and Datko*, 1987; *Tarboton et al.*, 1988; *Ijjasz-Vasquez et al.*, 1992; *Schorghofer and Rothman*, 2001, 2002]. These observations have led to suggestions that the physics that govern the development of erosional landforms are independent of spatial scale [e.g., *Somfai and Sander*, 1997].

Yet it has also been observed that landscapes have characteristic spatial scales. Field observations and measurements show that there is a limit to the erosional dissection of landscapes, in the sense that fluvial channels begin to form at scales much coarser than the granularity of the soil [*Gilbert*, 1877, 1909; *Horton*, 1945; *Montgomery and Dietrich*, 1992; *Dietrich and Montgomery*, 1998]. Studies that report self-similarity or self-affinity of topographic surfaces often note that this property only holds within a certain range of spatial wavelengths [*Church and Mark*, 1980; *Mark and Aronson*, 1984; *Gilbert*, 1989; *Moore et al.*, 1993; *Xu et al.*, 1993; *Evans and McClean*, 1995; *Gallant*, 1997; *Dodds and Rothman*, 2000]. Many landscapes also appear to contain quasiperiodic structures, including evenly spaced rivers and drainage basins [e.g., *Shaler*, 1899; *Hanley*, 1977; *Hovius*, 1996; *Talling et al.*, 1997; *Schorghofer et al.*, 2004]. For example, the landscape in Figure 1, part of the Gabilan Mesa, California, contains NW-SE-trending, first-order valleys with a remarkably uniform spacing.

The quasiperiodic valley spacing is visually striking. Is this merely a reflection of the human eye's affinity for organized patterns, or is it an important signature of the erosion processes that shaped the landscape? What is the "wavelength" of the ridges and valleys, and are they truly as nonrandom as they appear, or are they merely part of a continuum of scale-invariant landforms? Quantitative answers to these questions require a robust measurement technique that provides a statistical description of the topography.

Geomorphologists often use drainage density—defined as the total length of erosional channels per unit planform area—as a measure of the extent of landscape dissection. Despite recent advances that permit the calculation of drainage density as a continuous variable across a landscape [*Tucker et al.*, 2001], drainage density cannot provide answers to all of the questions posed above. Measuring drainage density requires the mapping of channels, a task that is difficult to perform without detailed field investigations [*Montgomery and Dietrich*, 1988; *Dietrich and Dunne*, 1993], and thus drainage density cannot be reliably calculated from topographic data alone. Furthermore, drainage density measures the extent of a drainage network, but provides no specific information about its structure. A topologically random drainage network can have the same drainage density as a network with evenly spaced channels. Even in a landscape with evenly spaced first-order channels, the inverse of drainage density and the average valley spacing will be comparable [*Horton*, 1932], but not necessarily equal.

If a landscape consists of well defined, parallel valleys, one can measure their spacing directly from topographic maps [e.g., *Hovius*, 1996; *Talling et al.*, 1997]. However, few landscapes have such simple structure. If valleys are not parallel, it is not obvious how or where their spacing should be measured. One therefore requires a robust measurement technique based on the overall shape of the topography rather than the planform geometry of the drainage network.

[1]Department of Earth & Planetary Sciences, Harvard University, Cambridge, MA, USA.

[2]Department of Earth & Planetary Science, University of California, Berkeley, CA, USA.

[3]Swiss Federal Institute for Forest, Snow, and Landscape Research (WSL), Birmensdorf, Switzerland.

[4]Department of Environmental Sciences, Swiss Federal Institute of Technology (ETH), Zürich, Switzerland.

0148-0227/08/$9.00

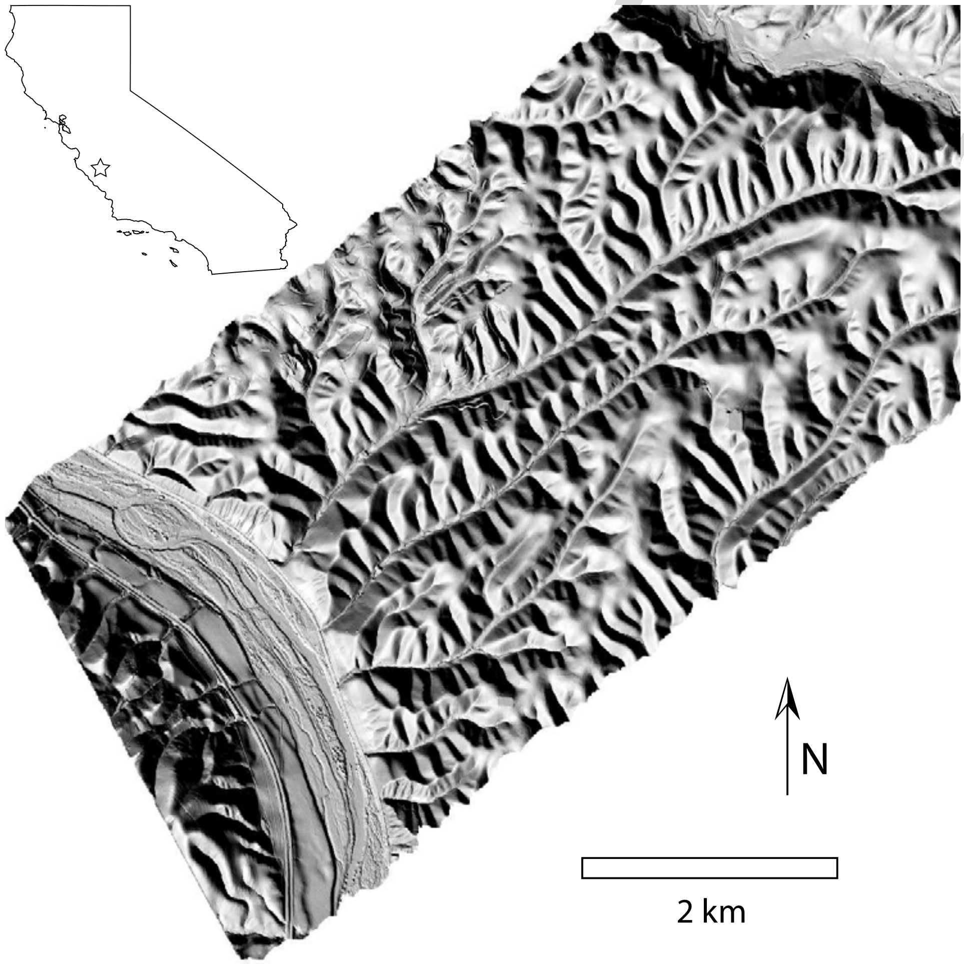

Figure 1. Shaded relief map of a portion of the Gabilan Mesa, California, at approximately 35.9°N, 120.8°W. The topographic data, with a horizontal resolution of 1 m, were collected and processed in 2003 by the National Center for Airborne Laser Mapping (NCALM). The Salinas River and U.S. Highway 101 are visible to the southwest.

Spectral analysis provides a means of measuring the strength of periodic (sinusoidal) components of a signal at different frequencies. The Fourier transform takes an input function in time or space and transforms it into a complex function in frequency that gives the amplitude and phase of the input function. If the input function has two or more independent dimensions, the Fourier spectrum gives amplitude and phase as a function of orientation as well as frequency.

A number of previous studies have used Fourier transforms to analyze topographic and bathymetric data. Some of these papers discuss the identification of periodic structures [*Rayner*, 1972; *Hanley*, 1977; *Stromberg and Farr*, 1986; *Ricard et al.*, 1987; *Mulla*, 1988; *Gallant*, 1997] or textures with preferred orientations [*Steyn and Ayotte*, 1985; *Mushayandebvu and Doucouré*, 1994], whereas others use the spectrum to describe the variance structure or scaling properties of the topography [e.g., *Steyn and Ayotte*, 1985; *Voss*, 1988; *Ansoult*, 1989; *Hough*, 1989; *Goff and Tucholke*, 1997]. Many of these studies used methods that were tailored to specific datasets or questions, and thus their procedures are not readily extendible to any topographic surface.

In this paper, we describe a general procedure for applying the two-dimensional, discrete Fourier transform to topographic data. We introduce a statistical method that provides a means of measuring the significance, or degree of nonrandomness, of quasiperiodic structures. By applying this procedure to two topographic datasets, we show that there are strong periodicities at certain scales, rather than a continuous distribution of spectral power across all scales, and that topographic roughness declines sharply below a certain spatial scale. We illustrate a filtering procedure that can be used to isolate the different frequency components of a topographic surface, and can thereby provide a means of measuring topographic attributes at certain scales and orientations. We conclude by discussing the implications of our results for fractal descriptions of landscapes.

2. Methods

2.1. The two-dimensional discrete Fourier transform

The discrete Fourier transform (DFT) of a two-dimensional dataset $z(x,y)$ consisting of $N_x \times N_y$ measurements spaced at even intervals Δx and Δy can be written [*Priestley*, 1981; *Percival and Walden*, 1993]

$$Z(k_x,k_y) = \sum_{m=0}^{N_x-1} \sum_{n=0}^{N_y-1} z(m\Delta x, n\Delta y) e^{-2\pi i\left(\frac{k_x m}{N_x}+\frac{k_y n}{N_y}\right)}, \tag{1}$$

where k_x and k_y are the wavenumbers in the x (positive east) and y (positive north) directions, and m and n are indices in the z array ($x = m\Delta x$, $y = n\Delta y$). The complex DFT expresses the amplitude and phase of sinusoidal components of z. The DFT is an $N_x \times N_y$ array, and the wavenumbers are the indices of the array. If z is real, the DFT is symmetric, and all the information is contained in any two adjacent quadrants of the DFT array. The output of most algorithms that compute the DFT must be rearranged to place the zero wavenumber element near the center of the array. Provided N_x and N_y are even, dividing the output array into four equal quadrants and exchanging the non-adjacent quadrants will place the zero wavenumber element at the position $(N_x/2+1, N_y/2-1)$ in the new array. If the wavenumbers are referenced to this location, an element at (k_x, k_y) in the DFT array corresponds to the two orthogonal frequency components

$$f_x = \frac{k_x}{N_x \Delta x}\,, \quad f_y = \frac{k_y}{N_y \Delta y}\,, \tag{2}$$

and the ranges of the wavenumbers are $-N_x/2 \leq k_x \leq N_x/2-1$ and $-N_y/2-1 \leq k_y \leq N_y/2$. If x and y have units of length, as in the case of topographic data, f_x and f_y have units of cycles per unit length. The Nyquist frequency, the highest frequency that can be resolved by data with a spacing Δ, is $(2\Delta)^{-1}$. Note that, for two-dimensional data arranged on a rectangular grid, Δ and the Nyquist frequency vary with orientation.

The 2D DFT provides information about orientation as well as frequency. The element at $Z(k_x, k_y)$ describes a wave with a wavelength

$$\lambda = \frac{1}{\sqrt{f_x^2 + f_y^2}}\,, \tag{3}$$

and an orientation θ, measured counterclockwise from the positive x direction (east) and given by

$$\tan\theta = \frac{k_y \Delta y}{k_x \Delta x}\,. \tag{4}$$

The quantity $\sqrt{f_x^2 + f_y^2}$ is often referred to as the radial frequency, and will be denoted here by f. Note that a two-dimensional wave with orientation θ has crests and troughs that trend perpendicular to θ. This distinction becomes particularly important when interpreting the spectral signatures of ridge-and-valley structures in topographic surfaces. All orientations discussed here refer to the orientation of the wave, which is orthogonal to the trend of ridges and valleys.

The power spectrum provides a measure of how the variance of z varies with frequency. One common way of estimating the power spectrum is the DFT periodogram:

$$P_{\mathrm{DFT}}(k_x, k_y) = \frac{1}{N_x^2 N_y^2} |Z(k_x, k_y)|^2\,. \tag{5}$$

The DFT periodogram has units of amplitude squared. It is linearly related to the power spectral density (PSD), which has units of amplitude squared per unit x frequency per unit y frequency, or amplitude squared per frequency squared: $P_{\mathrm{PSD}}(f_x, f_y) = P_{\mathrm{DFT}}(k_x, k_y) \cdot N_x N_y \Delta x \Delta y$. Parseval's theorem states that the sum of the P_{DFT} array (or, equivalently, the integral with respect to frequency of the P_{PSD} array) is equal to the variance of z. The root-mean-square amplitude A of the frequency components of z represented by a subset of the P_{DFT} array is

$$A = 2\sqrt{\Sigma P_{\mathrm{DFT}}}\,, \tag{6}$$

where ΣP_{DFT} is the sum of all the elements of the subset. The factor of 2 accounts for the fact that the DFT array is symmetric, with each signal appearing at both positive and negative frequencies. Because many natural signals, including ridges and valleys, are neither perfectly sinusoidal nor perfectly periodic (or have frequencies that fall between the discretely sampled frequencies in the DFT), their spectral signature is often spread over a range of frequencies. Thus, in practice, the reconstruction of amplitude usually requires summation over several adjacent elements that define a peak in the P_{DFT} array.

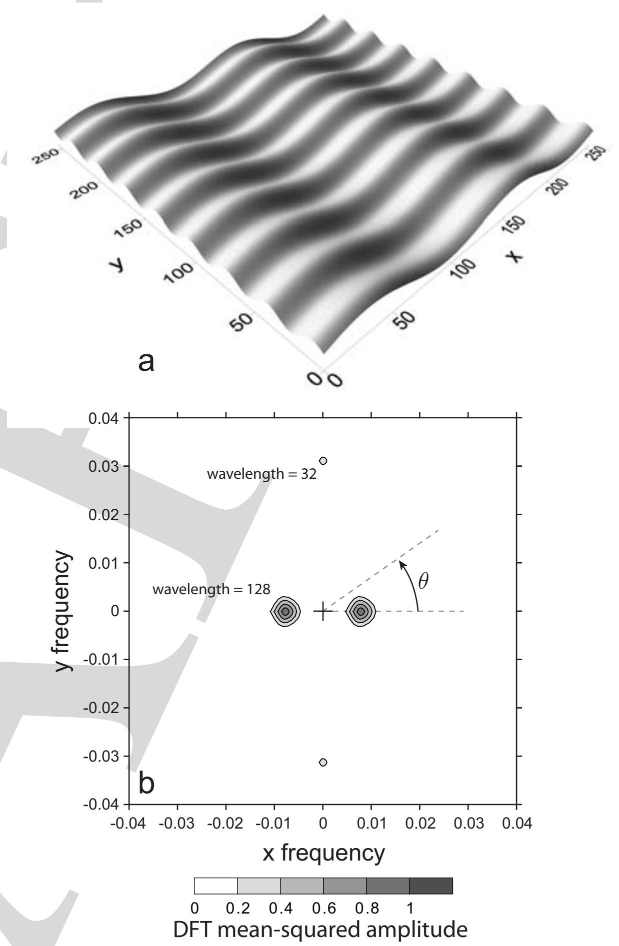

Figure 2. (a) A surface consisting of two orthogonal sine waves: one with a wavelength of 128 in the x-direction, the other with a wavelength of 32 in the y-direction and half the amplitude of the first. (b) A contour map of its power spectrum. The two peaks aligned in the x-direction ($\theta = 0°$) correspond to the lower-frequency (longer wavelength) signal, and therefore are closer to the origin; the peaks aligned in the y-direction ($\theta = 90°$) correspond to the higher-frequency (shorter wavelength) signal, and therefore are further from the origin. The crosshairs mark the zero-frequency origin, and the dashed angle illustrates how θ is measured.

Figure 2 illustrates the relationship between a two-dimensional surface and its power spectrum. The input signal (Figure 2a) consists of two orthogonal sine waves. The wave in the x-direction has a wavelength four times as long, and an amplitude twice as large, as the wave in the y-direction. The DFT periodogram (Figure 2b) contains two sets of peaks that are symmetrical about the zero frequency element at the center of the plot. Frequency is inversely proportional to wavelength, so the peaks that align in the y-direction are four times farther from the cross-hairs at zero frequency than those that align in the x-direction, which correspond to a signal with a wavelength four times as long. Because spectral power is a measure of mean squared amplitude, the peaks that align in the y-direction are one-fourth as high as those that align in the x-direction, which correspond to a signal with twice the amplitude. The two components of the input signal are perfect sinusoids with frequencies that correspond exactly to two of the discretely sampled frequencies in the DFT array, and so the spectral power in each peak is contained within a single element of the array (the spectrum in Figure 2b has been smoothed to make the peaks more easily visible).

2.2. Spectral analysis of topographic data: preprocessing steps

The Fourier transform makes assumptions about the input signal $z(x, y)$ that are violated by typical topographic data. Special processing procedures are therefore necessary to reduce effects that can contaminate the power spectrum. The Fourier transform treats the input signal as though it is stationary, with the same mean, variance, and frequency content throughout the sampled interval. Few natural signals are strictly stationary [*Weedon*, 2003], but the power spectrum provides a useful description of a signal if its mean and variance are roughly constant [*Priestley*, 1981]. To remove any spatial trends in the mean of a topographic dataset, a linear function in x and y (i.e., a plane) is fit to the input signal, z, and then subtracted from z.

The Fourier transform also assumes that the input signal is periodic at the edges of the sampled interval. If this is not the case, sinusoids at many different frequencies are required to describe the edge discontinuities, and these spurious signals will contaminate the power spectrum [*Priestley*, 1981; *Percival and Walden*, 1993]. This phenomenon is known as spectral leakage, and its effects can be mitigated with a two-step procedure. The linear detrending step described above reduces the magnitude of the edge discontinuity. The detrended signal is then multiplied by a window function, W, that has a maximum at its center and tapers smoothly to zero at its edges. Several simple window functions are suitable for most practical applications [see §13.4 of *Press et al.*, 1992]. We use a Hann (raised cosine) window, which for each array element (m, n) is given by

$$
\begin{aligned}
W(m,n) &= \begin{cases} \frac{1}{2}\left(1+\cos\frac{\pi r}{r'}\right) & r \le r' \\ 0 & r > r' \end{cases} \\
r^2 &= (m-a)^2 + (n-b)^2 \\
r'^2 &= \frac{a^2 b^2}{b^2\cos^2\theta + a^2\sin^2\theta} \\
a &= \frac{N_x - 1}{2} \quad ; \quad b = \frac{N_y - 1}{2} \\
\tan\theta &= \frac{n-b}{m-a} \,. \qquad (7)
\end{aligned}
$$

The normalization of the power spectrum can be modified to account for the change in variance that occurs when the input signal z is multiplied by the window function. For any two-dimensional window function $W(m, n)$, equation 5 becomes [*Press et al.*, 1992, §13.4]

$$
P_{\mathrm{DFT}}(k_x, k_y) = \left(N_x N_y \sum_{m=0}^{N_x-1} \sum_{n=0}^{N_y-1} W(m,n)^2 \right)^{-1} |Z(k_x, k_y)|^2 \,. \qquad (8)
$$

This normalization ensures that the sum of the elements in the P_{DFT} array will equal the variance of the detrended dataset $z(x, y)$, consistent with Parseval's theorem.

The most efficient algorithm for calculating the DFT of large topographic datasets is the fast Fourier transform (FFT), the most commonly used version of which is the algorithm of *Cooley and Tukey* [1965]. The efficiency of this algorithm is greatest when N_x and N_y are integer powers of two. This can be achieved by padding the windowed data with zeros, and the zero padding should be considered part of the window function W when applying equation 8.

2.3. Significance levels

In addition to providing information about the wavelength and orientation of periodic components of a topographic surface, the power spectrum can be used to assess the significance of these components. We are particularly interested in obtaining a measure of the degree of nonrandomness of a particular component; more formally, we seek the confidence level at which we can reject the null hypothesis that an observed periodic signal has occurred by chance in a random topographic surface. Given an estimate of the mean or background spectrum of a topographic surface, $\bar{P}(f)$, and the measured value of the power spectrum at a given frequency, this confidence level corresponds to the probability that the spectrum of a random surface will exceed the background by the observed amount at that frequency. If the Fourier coefficients (and therefore the amplitude and phase of the various frequency components) are assumed to be random, normally distributed variables, then the spectral power at a given frequency will be χ^2 distributed with two degrees of freedom [*Jenkins and Watts*, 1968]. The spectral power corresponding to a confidence level α is [*Gilman et al.*, 1963; *Percival and Walden*, 1993; *Torrence and Compo*, 1998]

$$
P_\alpha(f) = \frac{1}{2}\chi_2^2(\alpha)\bar{P}(f) \,, \qquad (9)
$$

where $\chi_2^2(\alpha)$ is the value at which the χ^2 cumulative distribution function with 2 degrees of freedom equals α. The method used to estimate the background spectrum $\bar{P}(f)$ is described in section 3.1.

Even if the power at a given frequency exceeds the significance level calculated from Equation 9, it is possible that the observed peak is a chance occurrence. Indeed, some "false positives" are to be expected if the spectral power at each frequency is χ^2-distributed: for example, 5% of the sampled frequencies in the spectrum of a random surface should exceed the 95% significance level ($\alpha = 0.95$). It is therefore also important to examine the distribution of significance over the spectrum. If signals that exceed the significance level are clustered together in space, orientation, or both, the observed peaks are less likely to be spurious.

The width of a spectral peak reflects the degree to which a feature is periodic and sinusoidal, because quasiperiodic or non-sinusoidal features must be described by a range of frequencies. Peak width (for example, the full width at half of the peak maximum) can therefore provide an estimate of the variability in a quasiperiodic structure, in a manner analogous to a standard deviation. Because frequency and wavelength are inversely proportional, this uncertainty envelope will not necessarily be symmetric about the peak value in the spatial domain.

3. Application to high-resolution topographic data

3.1. Measuring quasiperiodic topographic structures

The techniques described in section 2 can be used to test the assertion that landscapes are scale-invariant, random surfaces, and to describe quantitatively any quasiperiodic structures. We analyzed the spectra of two topographic datasets, one from the Gabilan Mesa, California, a landscape with characteristic spatial scales that are immediately obvious to the eye (Figure 3a), and another from the South

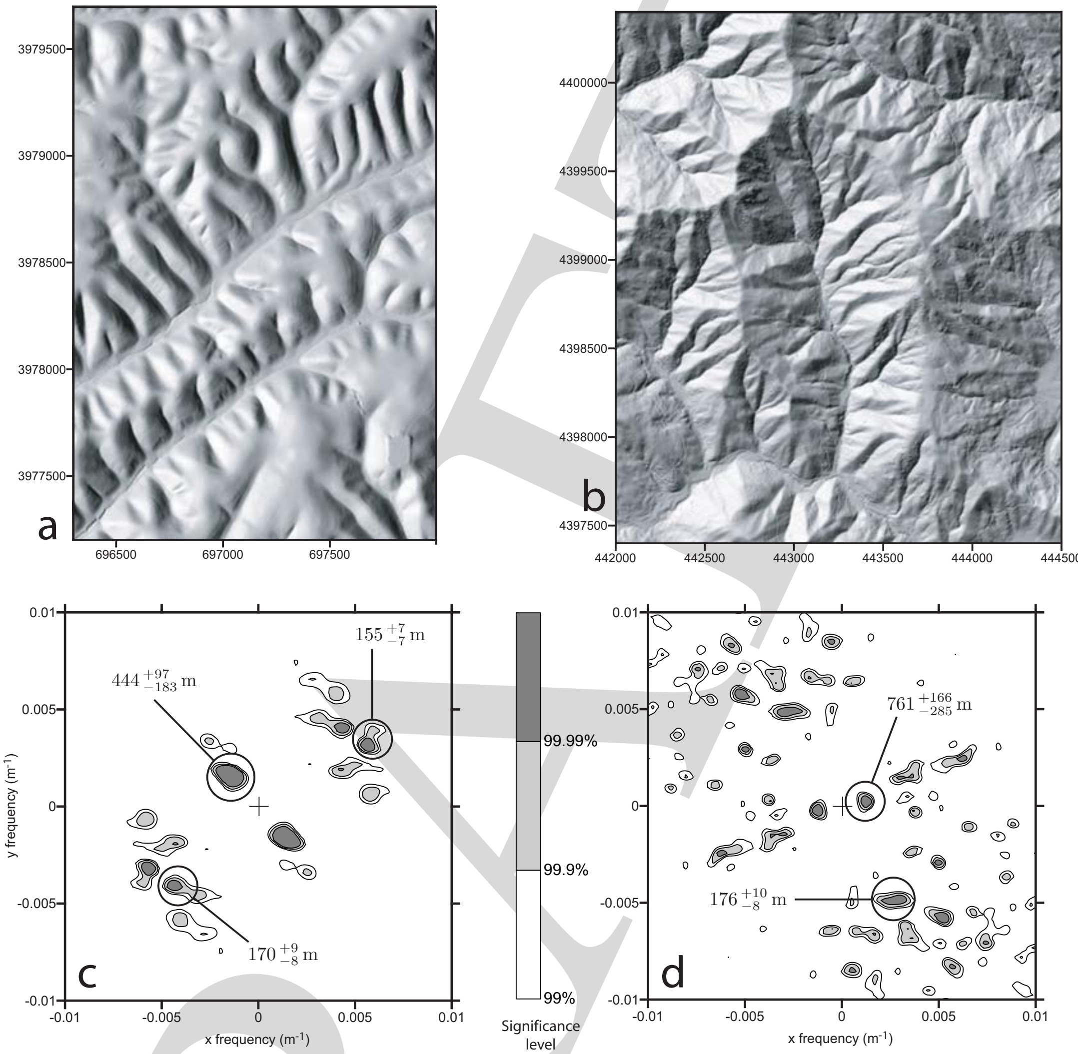

Figure 3. Shaded relief maps of (a) a subregion of the Gabilan Mesa, California, the landscape shown in Figure 1, with illumination from the left, and (b) part of the South Fork Eel River watershed, California, with illumination from the upper left. Grid spacing of the elevation data is 4 m. The axes of both maps give zone 10 UTM coordinates in meters. (c,d) Portions of the normalized power spectra for the landscapes in (a) and (b), respectively, produced by dividing the spectra by the background spectra in Figures 4a–b. Wavelengths corresponding to the largest peaks, with uncertainties derived from the peak widths, are shown on each plot. Contours correspond to significance levels calculated from Equation 9. Crosshairs mark the zero-frequency origin. Note that wavelength (=1/frequency) decreases nonlinearly with distance away from the origin.

Fork Eel River, California, a landscape in which characteristic scales are less apparent (Figure 3b).

3.1.1. Topographic data

Both datasets are airborne laser swath maps with a vertical precision of < 10 cm. Prior to gridding, raw laser returns from vegetation were removed with a block-minimum filter [*Axelsson*, 1999; *Haugerud and Harding*, 2003]. The resulting bare-earth data density averages one return per square meter for the Gabilan Mesa, and 2.6 returns per square meter for the Eel River. (Gridded bare-earth data with 1 m resolution are available for the Eel River site in the data archive at http://www.ncalm.org.) The horizontal resolution of the gridded data was reduced to $\Delta x, \Delta y = 4$ m to improve computational efficiency. As we show below, this grid resolution easily resolves the shortest wavelengths in the topography with significant amplitude relative to the vertical precision. The grid resolution was reduced by discarding points rather than by averaging, because averaging has the undesirable effect of suppressing spectral power at high frequencies.

Like the larger section of the Gabilan Mesa shown in Figure 1, the topography of the subsection in Figure 3a is dominated by NE-SW-trending canyons with orthogonal, evenly spaced tributary valleys. The distance between the two main canyons is roughly 500 m, and the spacing of adjacent tributary valleys (or, equivalently, the width of the intervening hillslopes) is typically between 150 and 200 m. The topography of the Eel River site (Figure 3b) is less visually suggestive of characteristic scales than the Gabilan Mesa, though there does appear to be some regularity in the arrangement of kilometer-scale ridges and valleys. The orientations of ridges and valleys are also more variable than in the Gabilan Mesa.

3.1.2. One-dimensional power spectra

Two-dimensional power spectra were computed for both landscapes. Trends in spectral power with changing frequency are most easily visualized by plotting the DFT mean-squared amplitude against radial frequency, which collapses

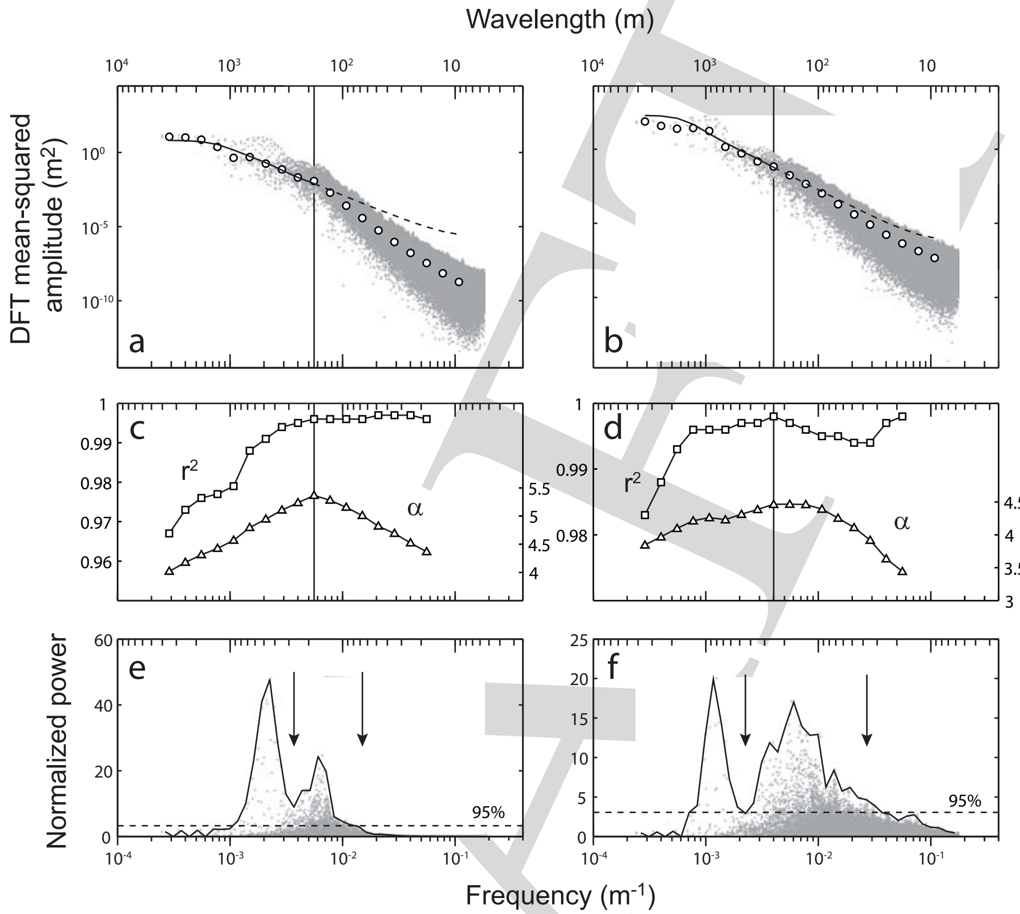

Figure 4. One-dimensional power spectra for (a) the Gabilan Mesa (Figure 3a) and (b) the Eel River (Figure 3b). Frequency (lower axis ticks on each plot) increases to the right, and wavelength (upper axis ticks) increases to the left. Each gray point is an individual element from the two-dimensional DFT array. Circles are the mean values within bins spaced logarithmically in frequency. Solid and dashed curves are background spectra estimated by averaging the spectra of randomly generated topographic surfaces with the same variance as the real data. The deviation of the background spectra from the binned values illustrates the roll-off in spectral power above the frequencies marked with vertical lines. Quantities used to identify these roll-off frequencies are plotted in (c) and (d). Note that the three highest values of α in (d) are identical. (e,f) normalized spectra produced by dividing the spectra in (a) and (b) by the background spectra. Solid lines showing the maximum values in 50 logarithmically spaced bins are included to highlight the upper envelopes of the normalized spectra. Dashed lines show significance levels calculated from Equation 9. Arrows mark the boundaries between frequency bands used to construct the filtered topography in Figure 5.

the two-dimensional spectra into one-dimensional plots (Figures 4a–b). Several interesting features are apparent in the spectra. In general, spectral power (and therefore amplitude) declines with increasing frequency, as is typically the case for landforms. At intermediate frequencies ($10^{-3}\,\mathrm{m}^{-1} \lesssim f \lesssim 10^{-2}\,\mathrm{m}^{-1}$), there are several broad peaks in the spectra that suggest departures from this trend. At higher frequencies, there is a marked steepening of the spectral slopes. The peaks and high-frequency roll-off are not artifacts of the processing procedure, as they are present in the spectra even when no detrending or windowing steps are performed. At lower frequencies, the spectral slope is gentler. This is due in part to the detrending of the topography prior to taking the DFT, which reduces the power at wavelengths comparable to the size of the sampled region, but a smaller reduction in spectral slope at long wavelengths is observed even if no preprocessing steps are applied.

The frequency at which the spectral roll-off occurs was identified for each spectrum by fitting least-squares regression lines to the log-transformed, binned data in Figures 4a–b. Beginning with the lowest-frequency point, and subsequently moving through all the points, the line was fit to all points at frequencies greater than or equal to the present point. The roll-off frequency was identified as the point at which the magnitude of the regression line slope (α) reached a maximum, and above which the goodness of fit (r^2) reached a plateau (Figures 4c–d). This procedure yielded roll-off frequencies of $5.6 \times 10^{-3}\,\mathrm{m}^{-1}$ (wavelength = 180 m) for the Gabilan Mesa and $4.0\times10^{-3}\,\mathrm{m}^{-1}$ (wavelength = 250 m) for the Eel River.

3.1.3. Background spectra and significance levels

To assess the significance of the peaks observed at intermediate frequencies in Figures 4a–b, it is necessary to estimate the background spectrum, $\bar{P}(f)$. The simplest approach would be to use the binned values as a representative mean spectrum, but these values are biased by the peaks. A better alternative is to use the mean spectrum of a random topographic surface with the same overall statistical properties as the real topography, but without a concentration of variance into any particular frequency bands. We used the diamond-square algorithm [*Fournier et al.*, 1982], a method commonly used to approximate fractal surfaces, to generate 1000 surfaces with the same variance (and therefore the same total spectral power) and grid dimensions as the topographic datasets, calculated the corresponding power spectra using the same processing technique applied to the real topography, and averaged the 1000 spectra. The roughness of the randomly generated surfaces, and therefore the spectral slope, is determined by a parameter H, which varies from 0 (roughest) to 1 (smoothest). For each landscape, we used the value of H that provided the best least-squares fit to the binned values below the roll-off frequency: $H = 0.8$ for the Gabilan Mesa, and $H = 0.9$ for the Eel River. These background spectra are plotted in Figures 4a–b. The divergence of the background spectra from the binned data at high frequencies highlights the roll-off in power in both spectra, and shows that it is more pronounced in the Gabilan Mesa than in the Eel River.

When the one-dimensional spectra are divided by the background spectra, deviations from the background are more apparent (Figures 4e–f). In both spectra, power is concentrated into two main peaks, which occur at wavelengths of roughly 450 m and 170 m for the Gabilan Mesa, and roughly 800 m and 170 m for the Eel River. All of these peaks exceed the 95% significance level calculated from Equation 9. Moreover, the concentration of spectral power into the frequencies surrounding these peaks (Figures 3c–d,4e–f) indicates that the apparent significance of the peaks is not spurious: 24% of the sampled frequencies below the roll-off exceed the 95% significance level for the Gabilan Mesa, and 14% for the Eel River, compared with the expected value of only 5% for a random surface. We can infer that the corresponding topographic structures are sufficiently periodic that they are unlikely to have occurred by chance in a random surface. The observation that the peaks in the Eel River spectrum exceed these significance levels by a smaller margin indicates that the ridges and valleys there are less periodic than in the Gabilan Mesa, consistent with the visual comparison between Figures 3a and 3b.

3.1.4. Two-dimensional power spectra

The two-dimensional spectra in Figures 3c–d reveal more about the geometry of these quasiperiodic structures, and provide estimates of the uncertainties in the measured wavelengths. The two-dimensional spectra were divided by two-dimensional versions of the background spectra in Figures 4a–b, a procedure analogous to that used to produce the normalized spectra in Figures 4e–f. The two large peaks in the Gabilan Mesa spectrum (Figure 3c) indicate a ridge-and-valley structure oriented at 139° E of N with a wavelength of $444\,^{+97}_{-183}$ m. (The uncertainty envelope corresponds to the full width, in the radial direction, of the spectral peak at half its maximum value.) This corresponds to the large, NE-SW-trending canyons in Figure 3a. As the map in Figure 3 suggests, these peaks are especially prominent because the width of the dataset spans only a few 444 m wavelengths, and therefore the signal appears very periodic. The smaller, higher-frequency peaks with the same orientation are harmonics of the main peak, a consequence of the non-sinusoidal shape of the ridges and canyons.

The paired clusters of five smaller peaks in Figure 3c are the spectral signature of the tributary valleys and the hillslopes that separate them. Because the hillslopes are lobate structures with a finite length (as opposed to infinitely long ridgelines, like the sinusoids in Figure 2), several superimposed groups of sine waves with slightly different orientations, amplitudes, and frequencies are required to describe their shape. The largest of these peaks corresponds to a signal oriented at 45° E of N with a wavelength of $170\,^{+9}_{-8}$ m, and the second largest to a signal oriented at 61° E of N with a wavelength of $155\,^{+7}_{-7}$ m. Pooling these two measurements yields an average spacing of $163\,^{+11}_{-11}$ m. The peaks corresponding to the 444 m and 163 m signals together account for 28% of the total variance in the detrended topography.

Peaks corresponding to quasiperiodic structures are easily recognized in the two-dimensional power spectrum for the Eel River site (Figure 3d), though the peaks are less prominent than those in the Gabilan Mesa spectrum. The two large peaks near the center show that the major ridges and valleys have a wavelength of $761\,^{+166}_{-285}$ m oriented 68° E of N. As in the Gabilan Mesa, smaller peaks with the same orientation are harmonics that reflect the non-sinusoidal shape of the ridges and valleys, but the harmonics in the Eel River spectrum are stronger because the ridges and valleys are more triangular in cross-section. Again, the main peaks corresponding to the large-scale ridges and valleys are strong because the dataset spans only a few wavelengths. The largest peaks in the orthogonal direction, which correspond to features with an orientation of 31° W of N and a wavelength of $176\,^{+10}_{-8}$ m, result from an abundance of roughly ENE-WSW-trending tributaries. Several frequency components with slightly different orientations are again required to describe the lobate geometry of the hillslopes separating the tributary valleys. Some of the smaller peaks at wavelengths of ∼150-200 m correspond to less numerous tributary valleys trending E-W or N-S. The peaks corresponding to the 761 m and 176 m signals together account for 29% of the total variance in the detrended topography.

3.2. Filtering

Having identified the portions of the power spectrum that correspond to various structures in the topography, we can isolate those structures for further analysis using a process known as Fourier filtering. The Fourier transform is reversible; that is, the original discrete function $z(x = m\Delta x, y = n\Delta y)$ can be recovered from its DFT $Z(k_x, k_y)$:

$$z(x,y) = \frac{1}{N_x N_y} \sum_{k_x=\frac{-N_x}{2}}^{\frac{N_x}{2}-1} \sum_{k_y=\frac{-N_y}{2}-1}^{\frac{N_y}{2}} Z(k_x,k_y) e^{2\pi i\left(\frac{k_x m}{N_x}+\frac{k_y n}{N_y}\right)} . \tag{10}$$

To reconstruct the portion of the topography that corresponds to certain frequency components of interest, one performs an inverse DFT on only those frequency components.

As an example, we used this filtering approach to separate the topography of the Gabilan Mesa and Eel River sites into components at three different scales. Using the normalized spectra in Figures 4e–f as a guide, we identified two frequencies for each landscape that bound the peak corresponding to the ∼170 m ridges and valleys, f_1 the lower frequency and f_2 the higher frequency. We then constructed three two-dimensional filter functions based on these frequencies: a low-pass filter, a band-pass filter, and a high-pass filter,

$$F_{\mathrm{low}} = \begin{cases} 1 & f < f_1 \\ \exp\left(\frac{-(f-f_1)^2}{2\sigma^2}\right) & f \geq f_1 \end{cases} \tag{11}$$

$$F_{\mathrm{band}} = \exp\left(\frac{-(f-\frac{1}{2}(f_1+f_2))^2}{2\sigma^2}\right) \tag{12}$$

$$F_{\mathrm{high}} = \begin{cases} \exp\left(\frac{-(f-f_2)^2}{2\sigma^2}\right) & f < f_2 \\ 1 & f \geq f_2 \end{cases} . \tag{13}$$

The edges of the low-pass and high-pass filters are radial Gaussian functions centered on f_1 and f_2, respectively, with standard deviations σ chosen to be $\frac{1}{3}|f_2 - f_1|$. The band-pass filter is a Gaussian centered halfway between f_1 and f_2, with $\sigma = \frac{1}{6}|f_2 - f_1|$. DFTs of the detrended, unwindowed

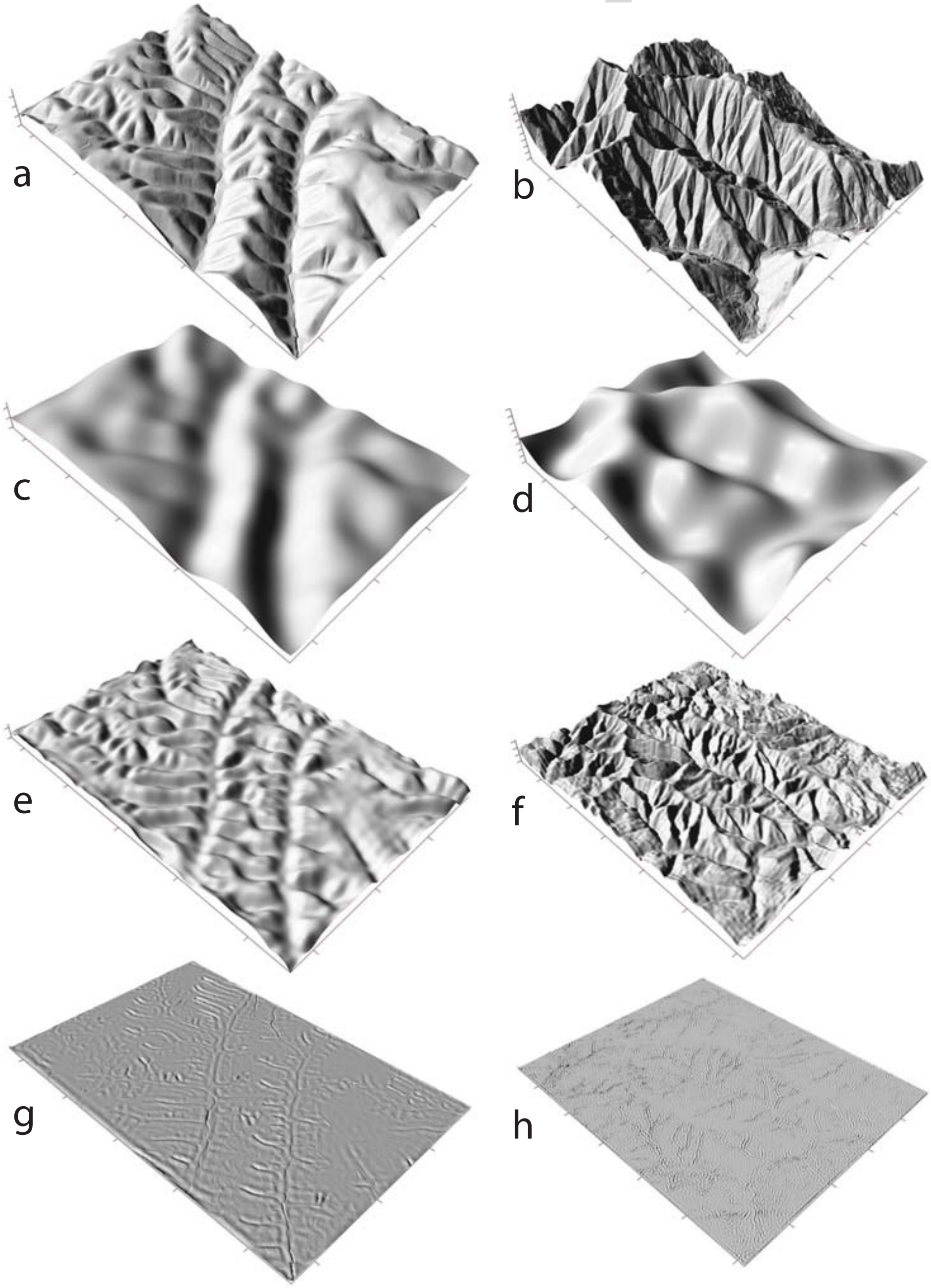

Figure 5. Perspective views of the landscapes shown in Figure 3 (a,b), and surfaces reconstructed from the frequency bands corresponding to larger valleys (c,d), smaller valleys (e,f), and small-scale roughness elements, including channel banks (g,h), using the filters in Equations 11–13. Frequency bands are indicated in Figures 4e–f. Horizontal tick interval is 500 m, vertical tick interval is 40 m. Vertical exaggeration is 2×.

topographic datasets were multiplied by the filter functions, and inverse DFTs were computed, yielding the surfaces in Figures 5c–h. This exercise confirms that the two sets of peaks in Figures 4e–f correspond to the roughly orthogonal ridge-valley structures observed in both landscapes. The remaining high-frequency components describe features that account for a small fraction of the total variance of the topography. These include sharp topographic discontinuities, such as channel banks and breaks in slope at the base of hillslopes, and minor roughness elements such as hummocky terrain on hillslopes and small measurement errors in the altimetry.

Fourier filtering offers a robust means of measuring topographic attributes at different scales. Using the filter $1 - F_{\mathrm{low}}(f)$, we removed the larger, ∼450 m ridges and valleys from the Gabilan Mesa, yielding the surface in Figure 6a. This surface allows us to create a continuous map of local relief at the scale of first-order drainage basins. At each location, the relief is taken to be four times the standard deviation of elevations within a 250 m radius. Four standard deviations was found to provide a close match to the total elevation range within each window, while still varying smoothly in space. Using the total range of elevations produces a discontinuous map, because it reflects only two elevations within each window location. The 250 m window radius was chosen because it is slightly larger than the mea-

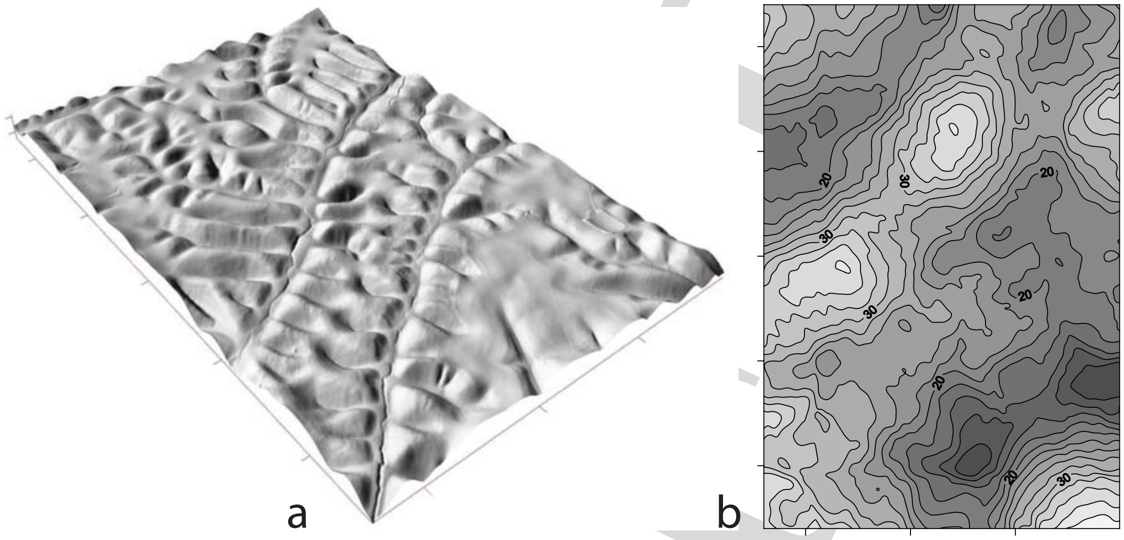

Figure 6. (a) Perspective view of the section of the Gabilan Mesa shown in Figure 3a, after the larger, ~450 m ridges and valleys have been removed with a spectral filter. (b) A continuous map showing the distribution of local relief at the scale of first-order drainage basins, created from the surface in (a). Contour interval is 2 m.

sured ridge-valley wavelength. The resulting map (Figure 6) shows trends in the local relief that are not obvious from visual inspection of the Gabilan Mesa topography in Figures 1, 3a and 5a.

4. Discussion

4.1. Deviations from fractal scaling

Having demonstrated the application of Fourier analysis to high-resolution topographic data and explored the information that can be extracted, we can return to the question of whether Earth has fractal surface topography. As noted in Section 1, previous authors using similar techniques have drawn the conclusion that topography is scale-invariant. In this section, we evaluate this conclusion by comparing our results with the predictions of the fractal model.

Landforms are generally larger in amplitude at longer wavelengths. The simplest spectrum with this property is a "red noise" spectrum with an inverse power-law dependence of spectral power on frequency: $P(f) \propto f^{-\beta}$. It is commonly reported that topographic spectra obey this relationship, and considerable attention has been devoted to interpretations of the exponent β [e.g., *Burrough*, 1981; *Mark and Aronson*, 1984; *Hough*, 1989; *Norton and Sorenson*, 1989; *Huang and Turcotte*, 1990; *Polidori et al.*, 1991; *Chase*, 1992; *Klinkenberg and Goodchild*, 1992; *Lifton and Chase*, 1992; *Ouchi and Matsushita*, 1992; *Xu et al.*, 1993; *Gallant et al.*, 1994; *Wilson and Dominic*, 1998]. In general, β reflects the rate at which the amplitudes of landforms decline relative to wavelength. For two-dimensional spectra, $\beta = 3$ indicates that amplitude is directly proportional to wavelength [*Voss*, 1988], such that landforms are self-similar, with a height-to-width ratio that is independent of scale. Other values of β imply that the topography is self-affine rather than self-similar: $\beta > 3$ indicates that shorter-wavelength features have smaller height-to-width ratios, and $\beta < 3$ indicates that shorter-wavelength features have larger height-to-width ratios. The exponent β is related to the fractal dimension, D, of the surface by [*Berry and Lewis*, 1980; *Saupe*, 1988; *Huang and Turcotte*, 1990]

$$D = \frac{8 - \beta}{2} \,. \qquad (14)$$

Note that these relationships apply to the spectra in Figures 4a–b because they are collapsed versions of two-dimensional spectra, as opposed to spectra derived from one-dimensional topographic profiles.

A topographic surface that is well described by the fractal model has some notable properties. First, the same scaling relationship between amplitude and wavelength should hold over all wavelengths. Second, the fractal dimension of a surface should lie within the range $2 \leq D \leq 3$. From Equation 14, the exponent β in the relationship $P(f) \propto f^{-\beta}$ should therefore lie within the range $2 \leq \beta \leq 4$. Third, there should be no concentration of variance into particular frequency bands, and therefore the topography should consist of landforms with a continuum of wavelengths.

The Gabilan Mesa and Eel River display several spectral characteristics that are inconsistent with the fractal model. First, the kink in the power spectrum, with a rapid decline of spectral power at higher frequencies (Figures 4a–b) implies a transition to a different scaling relationship between amplitude and wavelength at wavelengths less than ~143 m for the Gabilan Mesa, and ~200 m for the Eel River. At intermediate frequencies below this spectral roll-off, the spectral slopes for the Gabilan Mesa ($\beta = 2.8$) and the Eel River ($\beta = 3.1$) are close to 3, indicating that landforms have a nearly constant height-to-width ratio. Above the roll-off, the steeper spectral slopes ($\beta = 5.2$ and 4.5, respectively) indicate a height-to-width ratio that declines with increasing frequency. This does not imply that there are no topographic features at scales below the spectral roll-off, nor does it necessarily imply that dissection of the landscape by channel networks does not proceed at finer scales. It does imply that finer-scale features are much smoother than coarser-scale features. The observation that the break in spectral slope is larger for the Gabilan Mesa than for the Eel River suggests that short-wavelength features make a somewhat larger contribution to the topographic roughness at the Eel River, and that the transition from a landscape composed of ridges and valleys to one composed of relatively smooth hillslopes is more pronounced in the Gabilan Mesa.

Several previous studies have noted a similar decline in spectral power at short wavelengths, and although some of these conclude that it is probably an accurate reflection of the shape of the topography [*Culling and Datko*, 1987; *Gallant*, 1997; *Gallant and Hutchinson*, 1997; *Martin and*

Church, 2004], it is often interpreted as an artifact of topographic data interpolation [*Polidori et al.*, 1991; *Moore et al.*, 1993; *Gallant et al.*, 1994]. This clearly is not the case at the Gabilan Mesa or the Eel River sites, because the 4 m topographic data can resolve frequencies much higher than the roll-off frequency. Spectral evidence for a lower limit of topographic roughness may have been overlooked in the past because of the low spatial resolution of topographic data. The kink in the spectrum may not be as apparent in previously published spectra because it occurs at a frequency comparable to the Nyquist frequency of many topographic datasets. For a 30 m digital elevation map, for example, the shortest resolvable wavelength (equal to the inverse of the Nyquist frequency) is 60 m, which is only a factor of 2 to 3 smaller than the wavelengths at which the spectral transitions in Figures 4a–b occur. In contrast, the high-resolution data used here leave little doubt that the spectral kink represents a change in the character of the topography. This observation underscores the need for topographic data with a resolution sufficient to reveal landscape structure at scales significantly finer than that of first-order drainage basins.

It is sometimes suggested that a break in the scaling properties of a topographic surface indicates a transition from one suite of scale-invariant physical processes to another, with a resultant transition in the fractal dimension of the topography [e.g., *Huang and Turcotte*, 1990]. If we attempt to apply this concept to the topographic spectra presented here, we find a second way in which they are incompatible with the fractal model. As mentioned above, the exponent β for a fractal surface should lie between 2 and 4. Both the Gabilan Mesa ($\beta = 2.8$) and the Eel River ($\beta = 3.1$) satisfy this constraint at frequencies below the roll-off (though the range of frequencies below the roll-off is too narrow to give a clear fractal spectrum), but at frequencies above the roll-off, both spectra exhibit power-law scaling trends with $\beta > 4$. This demonstrates that both landscapes are smoother at fine scales than a two-dimensional random walk, inconsistent with fractal topography.

The characteristic of the two landscapes that is most at odds with the fractal model is the occurrence of quasiperiodic ridge-and-valley structures in the topography. The resulting concentration of power into specific frequency bands can appear small when spectra are plotted on logarithmic axes, particularly when spectral power spans many orders of magnitude, but the significance of the spectral peaks becomes more apparent when compared with an appropriate background spectrum (Figures 4e–f). Indeed, we have shown that much more variance is concentrated into these frequency bands than would be expected for a random surface.

Figures 4e–f also show a well-defined break between the spectral peaks associated with quasiperiodic structures at different wavelengths. The spectral decomposition illustrated in Figure 5 demonstrates that these peaks in the spectrum correspond to the roughly orthogonal ridges and valleys observed in the shaded relief maps of the topography. This is consistent with the visual impression that there is a break in scale between successive branches of the valley network in both landscapes.

The results presented here, which are based on only two study areas, do not necessarily indicate that the fractal model is inconsistent with all landscapes. Many landscapes have less uniform spacing of ridges and valleys than the Gabilan Mesa. The presence of complicating factors such as local tectonic deformation, heterogeneities in the strength or structure of bedrock and soil, or complex boundary conditions can obscure the characteristic scales that would otherwise emerge in an evolving landscape. For example, in the northwestern portion of the landscape in Figure 1, where several roads wind along the hillslopes, localized tectonic deformation has resulted in a pattern of landscape dissection that appears less periodic than the remainder of the terrain. In some cases, mechanisms such as bedrock jointing may introduce characteristic scales that differ from those expected from erosion processes alone.

Characteristic scales can emerge from erosion processes even in landscapes where significant heterogeneities exist, however. The steep terrain surrounding the South Fork Eel River is sculpted by debris flow scour, slope-dependent hillslope sediment transport, and deep-seated landsliding. The landslides disrupt the ridge-and-valley topography in many areas, leaving irregular topographic benches and discontinuous valleys. These effects are apparent in the eastern and northeastern portions of the area shown in Figure 3b. As we have shown here, characteristic scales still emerge in some parts of the landscape, but the prominence of deep-seated landsliding at the Eel River is probably one of the reasons why the topography there is less periodic than that of the Gabilan Mesa (section 3.1.3).

While the occurrence of characteristic scales in landscapes is by no means universal, our measurements imply that they might be present in landscapes that were previously thought to be scale-invariant. Field observations suggest that quasiperiodic structures are common in landscapes in which erosion processes, substrate properties and tectonic forcing are spatially uniform. In the Gabilan Mesa, for instance, the topography has been produced by the dissection of poorly consolidated Plio-Pleistocene sediments with bedding planes parallel to the original mesa surface. These sediments and the granitic basement beneath them have been uplifted with minimal local deformation, and the base level for the Mesa is set by the incision of the Salinas River to the southwest [*Dohrenwend*, 1975; *Dibblee*, 1979]. Models of long-term landscape evolution, which explore the interactions of erosion processes with simple tectonic forcing, geometrically simple boundary conditions, and spatially uniform substrate properties, support the idea that quasiperiodic landforms can develop under such conditions [e.g., *Howard*, 1994; *Kooi and Beaumont*, 1996; *Densmore et al.*, 1998; *Tucker and Bras*, 1998].

Such self-organized features inspired some of the earliest hypotheses about landscape evolution mechanisms. *Davis* [1892] and *Gilbert* [1909] suggested that the transition from hillslopes to valleys is controlled by a transition in process dominance from slope-dependent transport (creep) at small scales to overland flow transport at larger scales, an idea that was expounded on quantitatively by *Kirkby* [1971]. *Smith and Bretherton* [1972] and others extended this idea of a process competition to the incipient development of spatially periodic landforms, but these studies did not make predictions that could be compared to field measurements. *Horton* [1945] introduced the idea that a threshold for overland flow erosion sets the scale of the hillslope-valley transition by creating a “belt of no erosion” on and around drainage divides.

In a separate manuscript [*Perron et al.*, 2008, submitted], we build on these previous analyses to investigate the origins of the characteristic scales documented here. Using a dimensional analysis approach combined with a numerical landscape evolution model, we demonstrate that the wavelength of quasiperiodic ridges and valleys depends on the spatial scale at which fluvial dissection gives way to smooth hillslopes and the relative rates of the dominant erosion and transport processes shaping soil-mantled landscapes like the Gabilan Mesa. Our analysis indicates that it is possible to derive quantitative estimates of long-term process rates by measuring characteristic scales of landscape self-organization.

4.2. Benefits and limitations of the Fourier transform

The examples we have presented demonstrate that spectral analysis is a robust means of analyzing topographic structures that are qualitatively apparent but difficult to measure objectively. One could use a map and ruler to measure the spacing of some of the subparallel valleys in the Gabilan Mesa, but such an approach involves an arbitrary choice of which valleys to measure, and is poorly suited to landscapes in which the ridges and valleys are not parallel. In contrast, spectral analysis provides the basis for a relatively simple, accessible measurement technique that (1) reflects the entirety of a sample of terrain rather than a few features selected because they are visually striking, (2) is sensitive to elevation in addition to the horizontal structure of the topography, (3) can be applied to landscapes with variable ridge and valley orientations, and (4) requires no subjective delineation of landscape elements, such as the extent of the channel network.

There are two main problems with the application of the discrete Fourier transform to topographic data. First, the data are usually non-stationary, even when periodicities are as pronounced as in the Gabilan Mesa. Indeed, nonstationarity of the signal may be one attribute of topography that contributes to apparent fractal scaling [*Hough*, 1989]. Second, topographic features such as ridges and valleys are not sinusoids, but instead have a complex shape that must be described by a range of frequencies.

Techniques have been developed to address these problems. The maximum entropy method [*Burg*, 1967, 1975; *Press et al.*, 1992, §13.7] is sometimes used to estimate the power spectrum of nonstationary datasets of short duration or small spatial extent. Wavelet transforms allow for a variety of non-sinusoidal basis functions, and were designed with nonstationary signals in mind. They have been applied in a variety of fields in which nonstationary signals are common [for reviews, see *Foufoula-Georgiou and Kumar*, 1994; *Kumar and Foufoula-Georgiou*, 1997], including topographic analysis [e.g., *Malamud and Turcotte*, 2001; *Lashermes et al.*, 2007]. A branch of wavelet analysis using basis functions better suited to topographic surfaces has been applied to one-dimensional topographic profiles [*Gallant*, 1997; *Gallant and Hutchinson*, 1997], and wavelets have proved useful for identifying morphologic transitions similar to those documented here [*Lashermes et al.*, 2007].

These techniques have limitations, however. The maximum entropy method is subject to the same effects of nonstationarity as DFTs, and so the lone advantage of the technique in this context is that it allows nonstationary datasets to be parsed into shorter segments for analysis. The results of wavelet transforms (particularly transforms of two-dimensional data) are more difficult to interpret than those of the Fourier transform, and the positive wavelet transforms that use basis functions modeled after landforms are nonreversible [*Gallant*, 1997; *Gallant and Hutchinson*, 1997], making filtering impossible. Our results demonstrate that by using the preprocessing steps described here, it is possible to make meaningful measurements with the discrete Fourier transform, which is relatively simple to apply, produces results that are easily interpreted, and can easily be extended to filtering applications. Use of the Fourier transform also facilitates comparisons with past research on the scaling properties of landscapes, many of which have been based on Fourier spectra.

4.3. Further applications in geomorphology

Spectral analysis of topography has several applications beyond those presented above. By performing DFTs within a moving window, it would be possible to map the spatial variability in landscape properties, such as the wavelength or significance level of quasiperiodic structures, in a manner analogous to that used to produce the continuous map of local relief in Figure 6. Spectral properties could provide a basis for comparing attributes of synthetic topography with those of natural landscapes. For instance, temporal variations in the power spectra of numerical or physical models of landscape evolution could be used to quantify the approach to a statistical steady-state when an exact steady state (fixed topography in which the erosion rate is spatially constant) is not observed. Laboratory experiments [e.g., *Hasbargen and Paola*, 2000; *Lague et al.*, 2003] have produced topographic surfaces that reach a mass-balance steady state, but in which elevation is not a constant function of position and time. Because the power spectrum contains no phase information, it should remain unchanged if the frequency content of the model landscape is the same, even if the positions of ridges and valleys are not fixed. Finally, the observation that much of the variance in high-resolution topographic data is concentrated in relatively narrow frequency bands highlights the potential for data compression techniques that store and transfer topographic information as a function in the frequency domain rather than in space, an approach analogous to widely-used compression standards for digital images [e.g., *Wallace*, 1991].

5. Conclusions

By analyzing two-dimensional Fourier spectra derived from high-resolution topographic maps, we have shown that landscapes' spectral characteristics can deviate in several important ways from the fractal scaling that is often assumed to describe topographic surfaces. The spectra for two soil-mantled landscapes in northern California have transition frequencies above which spectral power declines more rapidly than is expected for a fractal surface, indicating that the topography is relatively smooth at finer scales. Each landscape also contains quasiperiodic ridge-and-valley structures in two distinct wavelength ranges. By comparing the measured spectra with spectra derived from synthetic surfaces, we have shown that these landforms are sufficiently periodic that they would be very unlikely to occur in a random surface. In both landscapes, the smallest of the quasiperiodic structures occurs at roughly the same wavelength as the roughness transition. This raises the possibility that the roughness transition and uniform valley spacing are signatures of the same mechanism, and that this mechanism operates at a characteristic spatial scale.

Acknowledgments. We thank the Orradre family of San Ardo, California, for granting access to their land. Airborne laser swath maps of the Gabilan Mesa and the Eel River were acquired through the National Center for Airborne Laser Mapping (http://www.ncalm.org) with support from the National Center for Earth-surface Dynamics (NCED). This work was supported by the Institute of Geophysics and Planetary Physics and a National Science Foundation Graduate Fellowship to JTP. Reviews by John Gallant, Sanjeev Gupta, and an anonymous referee led to several improvements in the manuscript. We thank Simon Mudd for his comments on an earlier draft.

References

Ahnert, F. (1984), Local relief and the height limits of mountain ranges, *American Journal of Science*, *284*(9), 1035–1055.

Ansoult, M. M. (1989), Circular sampling for fourier analysis of digital terrain data, *Mathematical Geology*, *21*(4), 401–410.

Axelsson, P. (1999), Processing of laser scanner data: algorithms and applications, *ISPRS Journal of Photogrammetry and Remote Sensing*, *54*(2), 138–147.

Balmino, G. (1993), The spectra of the topography of the earth, Venus, and Mars, *Geophysical Research Letters*, *20*(11), 1063–1066.

Berry, M. V., and Z. V. Lewis (1980), On the Weierstrass-Mandelbrot fractal function, *Proceedings of the Royal Society of London. Series A, Mathematical and Physical Sciences*, *370*(1743), 459–484.

Burg, J. P. (1967), Maximum entropy spectral analysis, in *Proceedings of the 37th Meeting of the Society of Exploration Geophysicists*, Oklahoma City.

Burg, J. P. (1975), Maximum entropy spectral analysis, PhD thesis, Stanford University.

Burrough, P. A. (1981), Fractal dimensions of landscapes and other environmental data, *Nature*, *294*(5838), 240–242.

Chase, C. G. (1992), Fluvial landsculpting and the fractal dimension of topography, *Geomorphology*, *5*(1-2), 39–57.

Church, M., and D. M. Mark (1980), On size and scale in geomorphology, *Progress in Physical Geography*, *4*(3), 342–390.

Cooley, J. W., and J. W. Tukey (1965), An algorithm for the machine calculation of complex Fourier series, *Mathematics of Computation*, *19*(90), 297–301.

Culling, W. E. H., and M. Datko (1987), The fractal geometry of the soil-covered landscape, *Earth Surface Processes and Landforms*, *12*, 369–385.

Davis, W. M. (1892), The convex profile of badland divides, *Science*, *20*, 245.

Davis, W. M. (1899), The geographical cycle, *The Geographical Journal*, *14*(5), 481–504.

Densmore, A. L., M. A. Ellis, and R. S. Anderson (1998), Landsliding and the evolution of normal-fault-bounded mountains, *Journal of Geophysical Research*, *103*(B7), 15,203–15,219.

Dibblee, T. W. (1979), Cenozoic tectonics of the northeast flank of the Santa Lucia Mountains from the Arroyo Seco to the Nacimiento River, California, in *Tertiary and Quaternary geology of the Salinas valley and Santa Lucia Range, Monterey County, California*, *Pacific Coast Paleogeography Field Guide*, vol. 4, edited by S. A. Graham, pp. 67–76, SEPM.

Dietrich, W. E., and T. Dunne (1993), The channel head, in *Channel Network Hydrology*, edited by K. Beven and M. J. Kirkby, pp. 175–219.

Dietrich, W. E., and D. R. Montgomery (1998), Hillslopes, channels, and landscape scale, in *Scale Dependence and Scale Invariance in Hydrology*, edited by G. Sposito, pp. 30–60, Cambridge University Press.

Dodds, P. S., and D. H. Rothman (2000), Scaling, universality, and geomorphology, *Annual Review of Earth and Planetary Sciences*, *28*(1), 571–610.

Dohrenwend, J. C. (1975), Plio-Pleistocene geology of the central Salinas Valley and adjacent uplands, Monterey county, California, PhD thesis, Stanford University.

Evans, I. S., and C. J. McClean (1995), The land surface is not unifractal: variograms, cirque scale and allometry, *Geomorph. NF Supp*, *101*, 127–147.

Foufoula-Georgiou, E., and P. Kumar (Eds.) (1994), *Wavelets in Geophysics*, Academic Press, New York.

Fournier, A., D. Fussell, and L. Carpenter (1982), Computer rendering of stochastic models, *Communications of the ACM*, *25*(6), 371–384.

Gallant, J. C. (1997), Scale and structure in landscapes, PhD thesis, Australian National University.

Gallant, J. C., and M. F. Hutchinson (1997), Scale dependence in terrain analysis, *Mathematics and Computers in Simulation*, *43*(3), 313–321.

Gallant, J. C., I. D. Moore, M. F. Hutchinson, and P. Gessler (1994), Estimating fractal dimension of profiles: A comparison of methods, *Mathematical Geology*, *26*(4), 455–481.

Gilbert, G. K. (1877), *Report on the Geology of the Henry Mountains*, U.S. Govt. Print. Office, Washington, D. C.

Gilbert, G. K. (1909), The convexity of hilltops, *J. Geol.*, *17*(4), 344–350.

Gilbert, L. E. (1989), Are topographic data sets fractal?, *Pure and Applied Geophysics*, *131*(1), 241–254.

Gilman, D. L., F. J. Fuglister, and J. M. Mitchell Jr (1963), On the power spectrum of red noise, *Journal of Atmospheric Science*, *20*(2), 182–184.

Goff, J. A., and B. E. Tucholke (1997), Multiscale spectral analysis of bathymetry on the flank of the Mid-Atlantic Ridge: Modification of the seafloor by mass wasting and sedimentation, *J. Geophys. Res*, *102*, 15,447–15,462.

Hanley, J. T. (1977), Fourier analysis of the Catawba Mountain knolls, Roanoke county, Virginia, *Mathematical Geology*, *9*(2), 159–163.

Hasbargen, L. E., and C. Paola (2000), Landscape instability in an experimental drainage basin, *Geology*, *28*(12), 1067–1070.

Haugerud, R. A., and D. J. Harding (2003), Some algorithms for virtual deforestation (VDF) of lidar topographic survey data, in *Proceedings of the ISPRS working group III workshop: 3-D reconstruction from airborne laser scanner and InSAR data*, Dresden, Germany.

Horton, R. E. (1932), Drainage basin characteristics, *Transactions of the American Geophysical Union*, *13*, 350–361.

Horton, R. E. (1945), Erosional development of streams and their drainage basins: hydrophysical approach to quantitative morphology, *Bull. Geol. Soc. Am*, *56*(3), 275–370.

Hough, S. E. (1989), On the use of spectral methods for the determination of fractal dimension, *Geophysical Research Letters*, *16*(7), 673–676.

Hovius, N. (1996), Regular spacing of drainage outlets from linear mountain belts, *Basin Research*, *8*, 29–44.

Howard, A. D. (1994), A detachment-limited model of drainage basin evolution, *Water Resources Research*, *30*(7), 2261–2286.

Huang, J. I. E., and D. Turcotte (1990), Fractal image analysis: Application to the topography of oregon and synthetic images, *Optical Society of America, Journal, A: Optics and Image Science*, *7*, 1124–1130.

Ijjasz-Vasquez, E. J., I. Rodríguez-Iturbe, and R. L. Bras (1992), On the multifractal characterization of river basins, *Geomorphology*, *5*, 297–310.

Jenkins, G. M., and D. G. Watts (1968), *Spectral analysis and its applications*, Holden-Day, San Francisco.

Kirkby, M. J. (1971), Hillslope process-response models based on the continuity equation, *Inst. Brit. Geogr. Spec. Publ.*, *3*, 15–30.

Klinkenberg, B., and M. F. Goodchild (1992), The fractal properties of topography: A comparison of methods, *Earth Surface Processes and Landforms*, *17*(3), 217–234.

Kooi, H., and C. Beaumont (1996), Large-scale geomorphology: classical concepts reconciled and integrated with contemporary ideas via a surface processes model, *J. Geophys. Res*, *101*(B2), 3361–3386.

Kumar, P., and E. Foufoula-Georgiou (1997), Wavelet analysis for geophysical applications, *Rev. Geophys.*, *35*(4), 385–412.

Lague, D., A. Crave, and P. Davy (2003), Laboratory experiments simulating the geomorphic response to tectonic uplift, *Journal of Geophysical Research*, *108*(B1), doi:10.1029/2002JB001785.

Lashermes, B., E. Foufoula-Georgiou, and W. E. Dietrich (2007), Channel network extraction from high resolution topography using wavelets, *Geophysical Research Letters*, *34*, L23S04, doi:10.1029/2007GL031140.

Lifton, N. A., and C. G. Chase (1992), Tectonic, climatic and lithologic influences on landscape fractal dimension and hypsometry: implications for landscape evolution in the San Gabriel Mountains, California, *Geomorphology*, *5*(1-2), 77–114.

Malamud, B. D., and D. L. Turcotte (2001), Wavelet analyses of Mars polar topography, *Journal of Geophysical Research*, *106*(E8), 17,497–17,504.

Mandelbrot, B. B. (1975), Stochastic models for the earth's relief, the shape and the fractal dimension of the coastlines, and the number-area rule for islands, *Proceedings of the National Academy of Sciences*, *72*(10), 3825–3828.

Mandelbrot, B. B. (1983), *The Fractal Geometry of Nature*, Freeman, New York.

Mark, D. M., and P. B. Aronson (1984), Scale-dependent fractal dimensions of topographic surfaces: An empirical investigation, with applications in geomorphology and computer mapping, *Mathematical Geology*, *16*(7), 671–683.

Martin, Y., and M. Church (2004), Numerical modelling of landscape evolution: geomorphological perspectives, *Progress in Physical Geography*, *28*(3), 317–339.

Matsushita, M., and S. Ouchi (1989), On the self-affinity of various curves, *Physica D: Nonlinear Phenomena*, *38*(1-3), 246–251.

Montgomery, D. R., and W. E. Dietrich (1988), Where do channels begin?, *Nature*, *336*, 232–234.

Montgomery, D. R., and W. E. Dietrich (1992), Channel initiation and the problem of landscape scale, *Science*, *255*(5046), 826–830.

Moore, I. D., A. Lewis, and J. C. Gallant (1993), Terrain attributes: Estimation methods and scale effects, in *Modeling Change in Environmental Systems*, edited by A. J. Jakeman, B. Beck, and M. McAleer, pp. 189–214, John Wiley and Sons.

Mulla, D. J. (1988), Using geostatistics and spectral analysis to study spatial patterns in the topography of southeastern Washington state, *USA Earth Surface Processes and Landforms*, *13*, 389–405.

Mushayandebvu, M. F., and C. M. Doucouré (1994), Regional crustal trends in South Africa from the spectral analysis of topographic and gravity data, *Journal of African Earth Sciences*, *19*, 27–27.

Newman, W. I., and D. L. Turcotte (1990), Cascade model for fluvial geomorphology, *Geophysical Journal International*, *100*, 433–439.

Norton, D., and S. Sorenson (1989), Variations in geometric measures of topographic surfaces underlain by fractured granitic plutons, *Pure and Applied Geophysics*, *131*(1), 77–97.

Ouchi, S., and M. Matsushita (1992), Measurement of self-affinity on surfaces as a trial application of fractal geometry to landform analysis, *Geomorphology(Amsterdam)*, *5*(1-2), 115–130.

Percival, D. B., and A. T. Walden (1993), *Spectral Analysis for Physical Applications*, Cambridge University Press.

Perron, J. T., W. E. Dietrich, and J. W. Kirchner (2008), Controls on the spacing of first-order valleys, *submitted to J. Geophys. Res.*

Polidori, L., J. Chorowicz, and R. Guillande (1991), Description of terrain as a fractal surface, and application to digital elevation model quality assessment, *Photogrammetric engineering and remote sensing*, *57*(10), 1329–1332.

Press, W. H., S. A. Teukolsky, W. T. Vetterling, and B. P. Flannery (1992), *Numerical Recipes in C: The Art of Scientific Computing*, Cambridge University Press, New York.

Priestley, M. B. (1981), *Spectral analysis and time series*, Academic Press, New York.

Rayner, J. N. (1972), The application of harmonic and spectral analysis to the study of terrain, in *Spatial Analysis in Geomorphology*, edited by R. J. Chorley, pp. 283–302, Methuen.

Ricard, Y., C. Froidevaux, and R. Simpson (1987), Spectral analysis of topography and gravity in the Basin and Range Province, *Tectonophysics*, *133*, 175–187.

Rodríguez-Iturbe, I., and A. Rinaldo (2001), *Fractal River Basins: Chance and Self-Organization*, Cambridge University Press.

Saupe, D. (1988), Algorithms for random fractals, in *The Science of Fractal Images*, edited by H. O. Peitgen and D. Saupe, pp. 71–113, Springer Verlag, New York.

Sayles, R. S., and T. R. Thomas (1978), Surface topography as a nonstationary random process, *Nature*, *271*(2), 431–434.

Schorghofer, N., and D. H. Rothman (2001), Basins of attraction on random topography, *Physical Review E*, *63*(2), 026112, doi:10.1103/PhysRevE.63.026112.

Schorghofer, N., and D. H. Rothman (2002), Acausal relations between topographic slope and drainage area, *Geophysical Research Letters*, *29*, 1633, doi:10.1029/2002GL015144.

Schorghofer, N., B. Jensen, A. Kudrolli, and D. H. Rothman (2004), Spontaneous channelization in permeable ground: theory, experiment, and observation, *Journal of Fluid Mechanics*, *503*, 357–374.

Shaler, N. S. (1899), Spacing of rivers with reference to the hypothesis of base-levelling, *Geol. Soc. Am. Bull.*, *10*, 263–276.

Shreve, R. L. (1966), Statistical law of stream numbers, *Journal of Geology*, *74*(1), 17–37.

Smith, T. R., and F. P. Bretherton (1972), Stability and the conservation of mass in drainage basin evolution, *Water Res. Res.*, *8*(6), 1506–1529.

Somfai, E., and L. M. Sander (1997), Scaling and river networks: A landau theory for erosion, *Physical Review E*, *56*(1), 5–8.

Steyn, D. G., and K. W. Ayotte (1985), Application of two-dimensional terrain height spectra to mesoscale modeling, *Journal of the Atmospheric Sciences*, *42*(24), 2884–2887.

Stromberg, W. D., and T. G. Farr (1986), A Fourier-based textural feature extraction procedure, *IEEE Transactions on Geoscience and Remote Sensing*, *24*, 722–731.

Talling, P. J., M. D. Stewart, C. P. Stark, S. Gupta, and S. J. Vincent (1997), Regular spacing of drainage outlets from linear fault blocks, *Basin Research*, *9*, 275–302.

Tarboton, D. G., R. L. Bras, and I. Rodríguez-Iturbe (1988), The fractal nature of river networks, *Water Resources Research*, *24*(8), 1317–1322.

Torrence, C., and G. P. Compo (1998), A practical guide to wavelet analysis, *Bulletin of the American Meteorological Society*, *79*(1), 61–78.

Tucker, G. E., and R. L. Bras (1998), Hillslope processes, drainage density, and landscape morphology, *Water Resources Research*, *34*(10), 2751–2764.

Tucker, G. E., F. Catani, A. Rinaldo, and R. L. Bras (2001), Statistical analysis of drainage density from digital terrain data, *Geomorphology*, *36*(3), 187–202.

Turcotte, D. L. (1997), *Fractals and Chaos in Geology and Geophysics*, Cambridge University Press.

Vening Meinesz, F. A. (1951), A remarkable feature of the Earth's topography, *Proc. K. Ned. Akad. Wet. Ser. B*, *54*, 212–228.

Voss, R. F. (1988), Fractals in nature: from characterization to simulation, in *The Science of Fractal Images*, edited by H. O. Peitgen and D. Saupe, pp. 21–70, Springer Verlag, New York.

Wallace, G. K. (1991), The JPEG still picture compression standard, *Communications of the ACM*, *34*(4), 30–44.

Weedon, G. P. (2003), *Time-Series Analysis and Cyclostratigraphy: Examining Stratigraphic Records of Environmental Cycles*, Cambridge University Press.

Wilson, T. H., and J. Dominic (1998), Fractal interrelationships between topography and structure, *Earth Surface Processes and Landforms*, *23*(6), 509–525.

Xu, T., I. D. Moore, and J. C. Gallant (1993), Fractals, fractal dimensions and landscapes: a review, *Geomorphology*, *8*(4), 245–262.

J. T. Perron (perron@eps.harvard.edu), Department of Earth & Planetary Sciences, 20 Oxford St., Cambridge, MA 02138, USA. J. W. Kirchner and W. E. Dietrich, Department of Earth & Planetary Science, 307 McCone Hall, Berkeley, CA 94720, USA.
The computer programs used to perform the analyses described in this paper are available from J.T.P.